Published in : Angewandte Chemie International Edition (2025), vol. 64, n°1, e202413605
DOI: https://doi.org/10.1002/anie.202413605
Status : Postprint (Author's version)

NONCONVENTIONAL FLUORESCENT NON-ISOCYANATE POLYURETHANE FOAMS FOR MULTIPURPOSE SENSING APPLICATIONS

Manas Mahapatra[a], Maxime Bourguignon[a], Bruno Grignard[a,c], Marylène Vandevenne[d], Moreno Galleni[d], and Christophe Detrembleur[a, b]

[a.] *Center for Education and Research on Macromolecules (CERM), CESAM Research Unit, Department of Chemistry, University of Liège, Liège, Belgium*
[b.] *WEL Research Institute, avenue Pasteur, 6, 1300 Wavre, Belgium*
[c.] *FRITCO2T Platform, CESAM Research Unit, University of Liege, Liege, Belgium*
[d.] *Laboratory of Enzymology and Protein Folding, Centre for Protein Engineering, InBioS, University of Liège, Liège, Belgium*

KEYWORDS :

non-isocyanate polyurethane foams, polyhydroxyurethane, nonconventional fluorescence, formaldehyde capture and detection, metal ions sensing, antibiotics detection

ABSTRACT :

Fluorescent foams with interconnected pores are attractive for the detection and quantification of various products. However, many fluorescent probes are suffering from aggregation-caused fluorescence quenching in their solid/aggregated state, are costly, and/or not straightforward to incorporate in foams, limiting their utility for this application. Herein, non-isocyanate poly-urethane foams, prepared by the simple water-induced self-blowing process, present a nonconventional fluorescence behaviour, i.e. they are intrinsically fluorescent with a multicolor emission without requiring ex situ traditional fluorescent probes. These foams demonstrate utility for capturing-sensing gaseous formaldehyde (an emblematic indoor air pollutant), as well as for detecting and quantifying various metal ions (Fe^{2+}, Cu^{2+}, Fe^{3+}, Hg^{2+}). They are also able to selectively sense tetracycline antibiotic in a ratiometric way with a high sensitivity. By exploiting the unique multicolor photoluminescent foam properties, a smartphone-compatible device is used for the facile antibiotic quantification. This nonconventional fluorescence behaviour is discussed experimentally and theoretically, and is mainly based on clusteroluminescence originating from multiple hydrogen bonding and hetero-atomic sub-luminophores, thus from aggregation-induced emission luminogens that are naturally present in the foams. This work illustrates that easily accessible non-conventional fluorescent NIPU foams characterized by a modular emission wavelength have an enormous potential for multiple substrates detection and quantification.

Published in : Angewandte Chemie International Edition (2025), vol. 64, n°1, e202413605
DOI: https://doi.org/10.1002/anie.202413605
Status : Postprint (Author's version)

1. Introduction

Fluorescent porous organic polymers emerged as the new generation of detection materials and sometimes quantification of various compounds, such as explosives, heavy metal ions and pesticides.[1-7] With an annual worldwide production of 12.7 MT,[8] polyurethane (PU) foams are major actors in the foam market, some of them finding utility as sensing materials when loaded by fluorescent probes.[9-14] For instance, fluorescent PU foams were reported for metal ions (e.g. Cu^{2+}, Fe^{3+}),[9-11] explosives (2,4,6-trinitrophenol, 2,4-dinitrotoluene)[12,13] or biomolecules (e.g. cysteine)[14] detection. These foams were obtained by the addition of the fluorophore in the foaming formulation or by post-foaming modification by the probe. Diverse fused aromatic rings,[12,13,15] lanthanides metal-ligand complexes,[9,16] organic dye,[11] metal nanoparticles,[14] or some metallic nanoclusters[17] were largely used as fluorescent probes. Many of them are however expensive[14] and/or toxic,[11] require multi-step synthesis to be produced,[9,13,16] and their incorporation in foams is not always straightforward. Moreover, some fluorophores are characterized by a single emission colour only,[9,10,15] which limited their sensing in a particular wavelength. When strong emission at the solid state (i.e. in solid foams) is targeted, aggregation-induced emission luminogens (AIEgens) were considered. They were extensively used in many luminescence-related areas such as bioimaging, theranostics,[18-22] organic light emitting diodes (OLEDs),[23,24] but also in foams for sensing applications.[12,13] These AIEgens are mostly aromatic-containing small molecules (e.g. triphenylamine, tetraphenylethylene,[19] hexaphenylsilole,[25,26] dihydroanthracene[22]) with an extended conjugated electronic structure. However, they suffer from similar drawbacks than conventional fluorophores, i.e. high cost, multistep synthesis, hydrophobicity, toxicity, and difficult incorporation to foams.[27-30]

Although the first reports date from the 90's for poly(amidoamine) (PAMAM) dendrimers,[31] purely aliphatic fluorescent polymers that do not contain any classical aromatic chromophores recently emerged as attractive alternatives to AIEgens-containing polymers for fluorescence-related applications.[30,32-39] Many of them are easily synthesized from more cost-effective widely available monomers, with multiple possible structure and properties variations. [33,34] The mechanism of nonconventional fluorescence is still debated, however, experimental results suggested that multiple hydrogen bonding and hetero-atomic aggregations between functional groups contributed significantly to clusteroluminescence.[40] The hetero-atomic sub luminophores, e.g. > C=O, —C≡N, —COOR, —$CONH_2$, —CONH—, —CON <, —NH_2, —NHR, —NR_2 and —NHOH, are not emissive in dilute solution, however, highly emissive in concentrated solution or in aggregated/clustered state.[28,33,35,36,40,41] Aggregations of these hetero-atomic subluminophores induced unprecedented fluorescence via restrictions of vibrionic and rotational motions which dimin-ished the nonradiative decays.[28,40] Although validated for some bulk polymers, there is no example of nonconventional fluorescence polymer foams, nor of their applications potential.

Recent REACH constraints regarding the utilization of toxic isocyanates for preparing PUs are pushing the search for non-isocyanate polyurethanes (NIPU).[42] Amongst the various strategies, the copolymerization of poly(cyclic carbonate)s with polyamines provided one of the most promising

Published in : Angewandte Chemie International Edition (2025), vol. 64, n°1, e202413605
DOI: https://doi.org/10.1002/anie.202413605
Status : Postprint (Author's version)

greener substitutes to conventional PUs, polyhydroxyurethanes (PHU). Importantly, the urethane and pending hydroxyl groups of the PHU backbone contributed to clusteroluminescence by multiple n-π* transitions between C=O···C=O and HO···C=O functional groups, and hydrogen bonding.[43-45] PHUs were thus characterized by a nonconventional fluorescence behaviour that was notably exploited for white or multi-colour LEDs,[23,24] cell culture and imaging,[46,47] and anti-counterfeiting ink.[45] Only one example reported the utilization of PHU solution for sensing Fe^{3+}.[46]

This study reports a new class of nonconventional fluorescent foams of the PHU-type, easy to prepare at large scale from cheap reagents (Scheme 1). The water-induced foaming process involved to produce the foams has the advantage to spontaneously bring additional alcohol functionalities to the polyurethane matrix, enhancing the clusteroluminescence and imparting unprecedented multicolour emission to the foams. These properties are exploited for sensing various species in a simple manner. Gaseous formaldehyde (an emblematic indoor air pollutant), various metal ions (e.g. Fe^{2+}, Cu^{2+}, Fe^{3+}, Hg^{2+}) but also an antibiotic (tetracycline) are captured, detected and for some of them, quantified by exploiting the modification of the foam's fluorescence properties. The origin of this fluorescence alteration is discussed based on experimental data and theoretical calculations. This work demonstrates that easily accessible non-isocyanate polyurethane foams (NIPUFs) present multicolour emissions that can be exploited for multipurpose sensing applications.

2. Results and discussion

2.1. NONCONVENTIONAL FLUORESCENT NON-ISOCYANATE POLYURETHANE FOAMS: PREPARATION AND FLUORESCENCE PROPERTIES

Non-isocyanate polyurethane foams (NIPUFs) were prepared by our recently reported[48] water-induced self-foaming strategy that consisted in adding water and a catalyst (KOH) to the NIPU formulation composed of a CO_2-based tricyclic carbonate and a polyamine (Scheme 1 and Table S1a). We selected this foaming procedure as it is easy to implement, is scalable and more importantly, yields NIPUFs presenting many hydroxyl groups and urethanes prone to multiple hydrogen bonding, expectedly favouring clusteroluminescence. Indeed, besides the aminolysis of the cyclic carbonate groups that provides the hydroxy-urethane linkages, their partial hydrolysis releases CO_2 as the blowing agent together with vicinal diols (Scheme 1). The latter are expected to further contributing to hydrogen bonding inside the PHU matrix.

In this work, three NIPUFs were prepared, all from the same tricyclic carbonate (trimethylolpropane triscarbonate, TMPTC), but a different polyamine following our established protocol, i.e. m-xylylene diamine (mXDA) (foam NIPUF1), 1,2-bis(2-aminoethoxy)ethane (EDR) (foam NIPUF2), and a mixture of EDR and polyethylene imine (PEI) (foam NIPUF3) (see ESI for details). Figure 1a summarizes the foams characteristics. In all cases, we produced crosslinked NIPUFs of open-cell morphology with a high gel content (> 90%) and a high thermal stability ($T_{d,10\%}$ > 265 °C) (Figure 1 and Figure S1a-S3a).

Published in : Angewandte Chemie International Edition (2025), vol. 64, n°1, e202413605
DOI: https://doi.org/10.1002/anie.202413605
Status : Postprint (Author's version)

Densities around 140 kg.m^{-3} were obtained for NIPUF1 and NIPUF2, and were higher for NIPUF3 (290 kg.m^{-3}) due to the structure of PEI that limited the foam expansion. High gel contents were also noted for all foams, attesting from their crosslinked nature (Figure 1a). After drying, the foams presented a glass transition temperature of 44.3 (NIPUF1), 8.4 (NIPUF2) and -2.9 °C (NIPUF3) (Figure S1b-S3b). Compression strain-stress curves revealed the rigid nature of NIPUF1 prepared from the aromatic diamine with a compression modulus (E) of 26.05 MPa, while foams prepared from aliphatic polyamines were flexible, i.e. NIPUF2 (E = 0.087 MPa) and NIPUF3 (E = 0.16 MPa) (Figure 1e-g). Both NIPUF2 and NIPUF3 foams recovered their shapes after compression beyond the elastic region.

The fluorescence emission spectra of the foams were monitored at different excitations wavelengths (λ_{ex}), from 330 to 500 nm, and are shown in Figure 2a-c. Importantly, all foams were emissive, with a maximum emission that depended on the foam and the excitation wavelength, i.e. at 510 nm for NIPUF1 (λ_{ex} = 460 nm), 490 nm for NIPUF2 (λ_{ex} = 430 nm) and 498 nm for NIPUF3 (λ_{ex} = 430 nm). As NIPUF1 was produced by using an amine bearing an aromatic moiety, the emission spectra of mXDA were monitored at these excitation wavelengths. Although this amine was slightly emissive at low λ_{ex}, almost no emission above 440 nm was observed (Figure S4), thus where NIPUF1 was highly emissive. This confirmed that mXDA was not responsible for the foam emission. Similar observations were done for TMPTC and PEI (Figure S4). For NIPUF2 and NIPUF3 where no aromatic compounds were present in the foams, high emissive materials were obtained too, further suggesting a non-conventional fluorescence behaviour in purely aliphatic systems. NIPUF2 showed brighter fluorescence as confirmed by the fluorescence quantum yield of 11.30 ± 0.14% (λ_{ex} = 430 nm) than that of NIPUF1 (5.41 ± 0.99% at λ_{ex} = 460 nm) and NIPUF3 (7.64 ± 0.97% at λ_{ex} = 430 nm) (Figure S5). The observation of the excitation wavelength dependent emission for all foams suggested that multiple emission states were present. The consequence is that the emission wavelength of the foams can simply be tuned in the blue-to-red region by varying the excitation wavelength as shown on the CIE colour space diagrams (Figure 2d-f and Table S2). This unique multicolour emission was further illustrated by imaging the foams under different excitation wavelengths. As shown in Figure 2g, their color changed from bright cyan, green, yellowish green, yellow, red and deep red when excited at 454, 488, 514, 543, 594 and 633 nm, respectively.

It has to be noted that NIPUF1 showed enhanced fluorescence intensity and higher emission wavelength as compared to NIPUF2. The extra rigidity in NIPUF1, coming from the used aromatic mXDA, was assumed to be responsible for this effect (T_g = 44.3 °C for NIPUF1 *vs* 8.4 °C for NIPUF2). Along with rigidity, the electronic effects of the aromatic group (π-π stacking, n-π* transition) were expected to contribute to emission wavelength too. To give some clues to this statement, we prepared a NIPU foam containing rigid cyclohexane units instead of benzyl ones by substituting mXDA by 1,3-cyclohexanedimethanamine. The T_g of this foam (47.7 °C) was comparable to NIPUF1 (T_g = 44.3 °C), and showed hypsochromic shift (blue shift) of 84 nm in emission wavelength as compared to NIPUF1 as well as a less intense fluorescence (Figure S6). Therefore, the foam rigidity is not the sole parameter for controlling the fluorescence enhancement and shifting in emission wavelength.

Published in : Angewandte Chemie International Edition (2025), vol. 64, n°1, e202413605
DOI: https://doi.org/10.1002/anie.202413605
Status : Postprint (Author's version)

We also verified that the fluorescence spectra of the foams were not dependent on the foam density. This is illustrated in Figure S7, for NIPUF2 of different densities (160, 300 and 410 kg.m^{-3}), where their fluorescence spectra, recorded at λ_{ex} = 430 nm, were very similar in maximum emission wavelength. For sake of comparison, the fluorescence spectrum of NIPUF2 (λ_{ex} = 430 nm) was compared to those of commercially available medical grade isocyanate-based polyurethanes, i.e. thermoplastic Carbothane-TPU and thermoset PU foam (Suprasorb® P) (Figure S8). While Carbothane-TPU was not emissive, the Suprasorb® P-PU foam was slightly emissive, however blue shifted and of very low intensity compared to NIPUF2. This further suggested the additional participation of the pending OH groups of the polyhydroxyurethane structure of NIPUF2 to clusteroluminescence.

Fluorescence lifetime imaging microscopy (FLIM) that enables to identify the time elapsing between the excitation of the fluorophore, its emission and decay, was then used to examine the fluorophore's decay rate, and to obtain relevant information regarding the distribution of the fluorophores in the polymer matrix as well as to determine the nature of quenching (static or dynamic) when treated with guest molecules (see ESI for details). Figures 2h-j show the FLIM images of the three NIPUFs; the lifetime distributions were visualized from the scattered yellow, green and cyan dots. The foam walls were green-yellow coloured with a rather homogeneous distribution of the two colours (and thus lifetimes), attesting for an homogeneous distribution of the nonconventional fluorescent chromophores within the polymer matrix. The average lifetime values were 5.6 (for NIPUF1), 5.9 (for NIPUF2) and 5.7 ns (for NIPUF3), thus within the fluorescence range (see Figure S9 in ESI regarding the calculation of the lifetime values).

As NIPUFs did not contain any conventional fluorescent chromophores, we hypothesized that aggregates formed by multiple hydrogen bonding and/or hetero-atomic interactions present within the foams microstructure, e.g. —NHCOO—, —OH, —O— and —CH_2OH, were responsible for the clusteroluminescence (Figure 3a). Compared to NIPU unfoamed materials (synthesised from the same NIPU formulation but without water), the emissions of NIFUF2 and NIPUF3 were slightly red shifted of 12 and 14 nm, respectively (Figure S10), and the three NIPU foams showed enhanced emission suggesting the participation of additional groups to hydrogen bonding (e.g. vicinal diols) and thus to clusteroluminescence.

To further support this hypothesis, all possible aggregates were computed theoretically by density functional theory (DFT) and time dependent DFT (TDDFT) on model compounds that represent the main functional groups of NIPUFs expected to be involved in aggregations (see Figures S11-S26 in ESI for all details regarding the calculations).[49-51] In brief, the emissive nature of all NIPU foams were established by the lowering of HOMO—LUMO energy gaps in first excited state as compared to ground state (Figure 3b). The lowering of HOMO—LUMO energy gaps in ground state when moving from small-to-moderate-to-large clusters supported the red shifted emission, and thus the multicolour emission (Figure 3c,d). Moreover, TDDFT calculations evidenced the participation of all possible hydrogen bonding to aggregation, and confirmed that the fluorescence was raised from the through space n-π* conjugations (TSC) of chromophores (—NHCOO—, —OH, —O—, —CH_2OH, etc.) within the hydrogen-bonded rigid microstructure of NIPU foams (Table S3-S5 and see ESI for

Published in : Angewandte Chemie International Edition (2025), vol. 64, n°1, e202413605
DOI: https://doi.org/10.1002/anie.202413605
Status : Postprint (Author's version)

details). In the case of NIPUF3, additional contributions to fluorescence originated from —NH— interactions.

We then evaluated the potential of NIPUF3 for sensing various pollutants, i.e. formaldehyde (FA, an emblematic indoor air pollutant), metal ions and antibiotics (both found in waste water). NIPUF3 was selected as PEI used for its preparation is well-known to react with formaldehyde and to complex metal ions.[52-60] We thus hypothesized that these reactions/interactions would affect the aggregations within the foams, and therefore the foam clusteroluminescence, enabling facile detection of these species.

Scheme 1. *Nonconventional fluorescent non-isocyanate polyurethane foams (NIPUFs) prepared by the water-induced self-foaming process and their use for multipurpose sensing applications.*

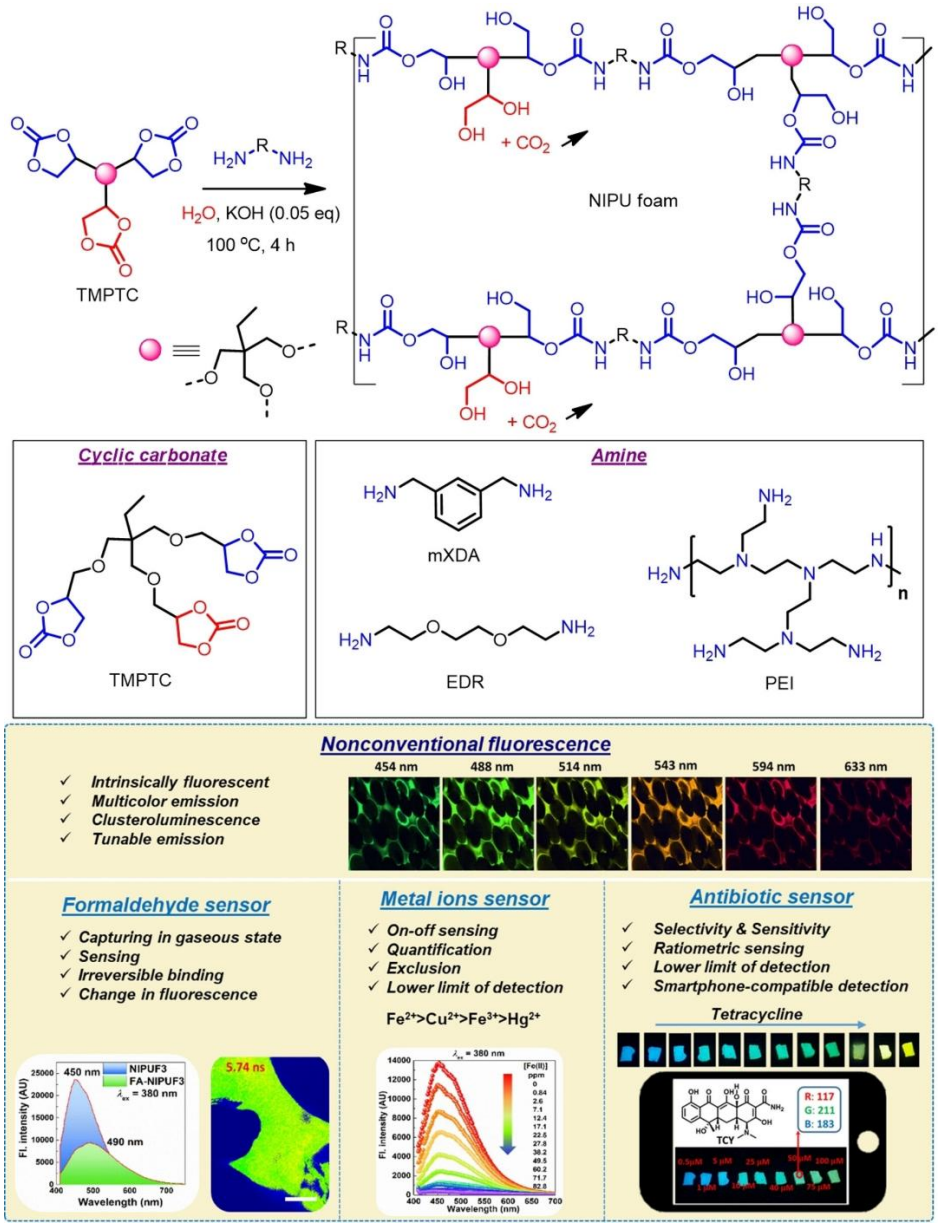

Published in : Angewandte Chemie International Edition (2025), vol. 64, n°1, e202413605
DOI: https://doi.org/10.1002/anie.202413605
Status : Postprint (Author's version)

***Figure 1**. (a) Formulation and properties of NIPU foams (mXDA: m-xylylene diamine; EDR: 1,2-bis(2-aminoethoxy)ethane; PEI: polyethyleneimine), photographic images and SEM photomicrographs (scale bar = 5 mm) of (b) NIPUF1, (c) NIPUF2 and (d) NIPUF3 and compressive stress-strain curves of (e) NIPUF1(E = 26.05 ±5.40 MPa), (f) NIPUF2 (E = 0.08 7±0.03 2 MPa) and (g) NIPUF3 (E = 0.16±0.026 MPa).*

(a) Name	Amine	Density [kg.m^{-3}]	Gel content [%]	T_g [°C]	$T_{d,10\%}$ [°C]
NIPUF1	mXDA	143 ± 13	96 ± 5.7	44.3	267
NIPUF2	EDR	142 ± 12	91 ± 2.5	8.4	265
NIPUF3	EDR + PEI	291 ± 15	93 ± 1.4	-2.9	265

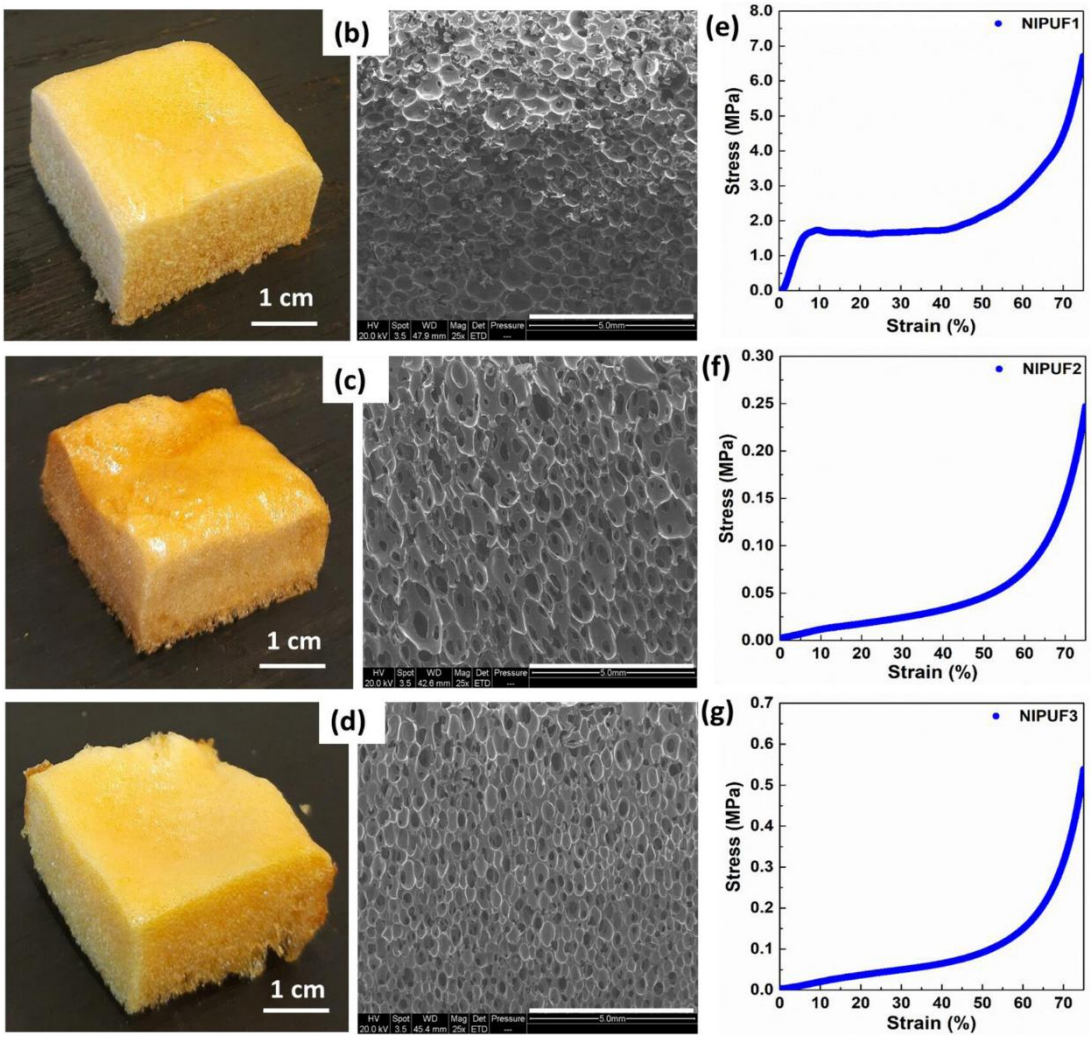

Published in : Angewandte Chemie International Edition (2025), vol. 64, n°1, e202413605
DOI: https://doi.org/10.1002/anie.202413605
Status : Postprint (Author's version)

***Figure 2**. Influence of amines and polyamine on the fluorescence of (a) NIPUF1, (b) NIPUF2 and (c) NIPUF3 prepared using water induced strategy; the Commission Internationale de l'éclairage (CIE) plots of (d) NIPUF1, (e) NIPUF2 and (f) NIPUF3; (g) confocal images of NIPU foams captured at different excitation wavelengths (454, 488, 514, 543, 594 and 633 nm), full Figure scale = 2400 μm; fluorescence lifetime imaging microscopy (FLIM) images of(h) NIPUF1, (i) NIPUF2 and (j) NIPUF3 showing different lifetimes, using the laser source of 455 nm, jet colormap is used for generating the image colormap, scale bar = 100 μm; the used threshold minimum/maximum = 100/5000.*

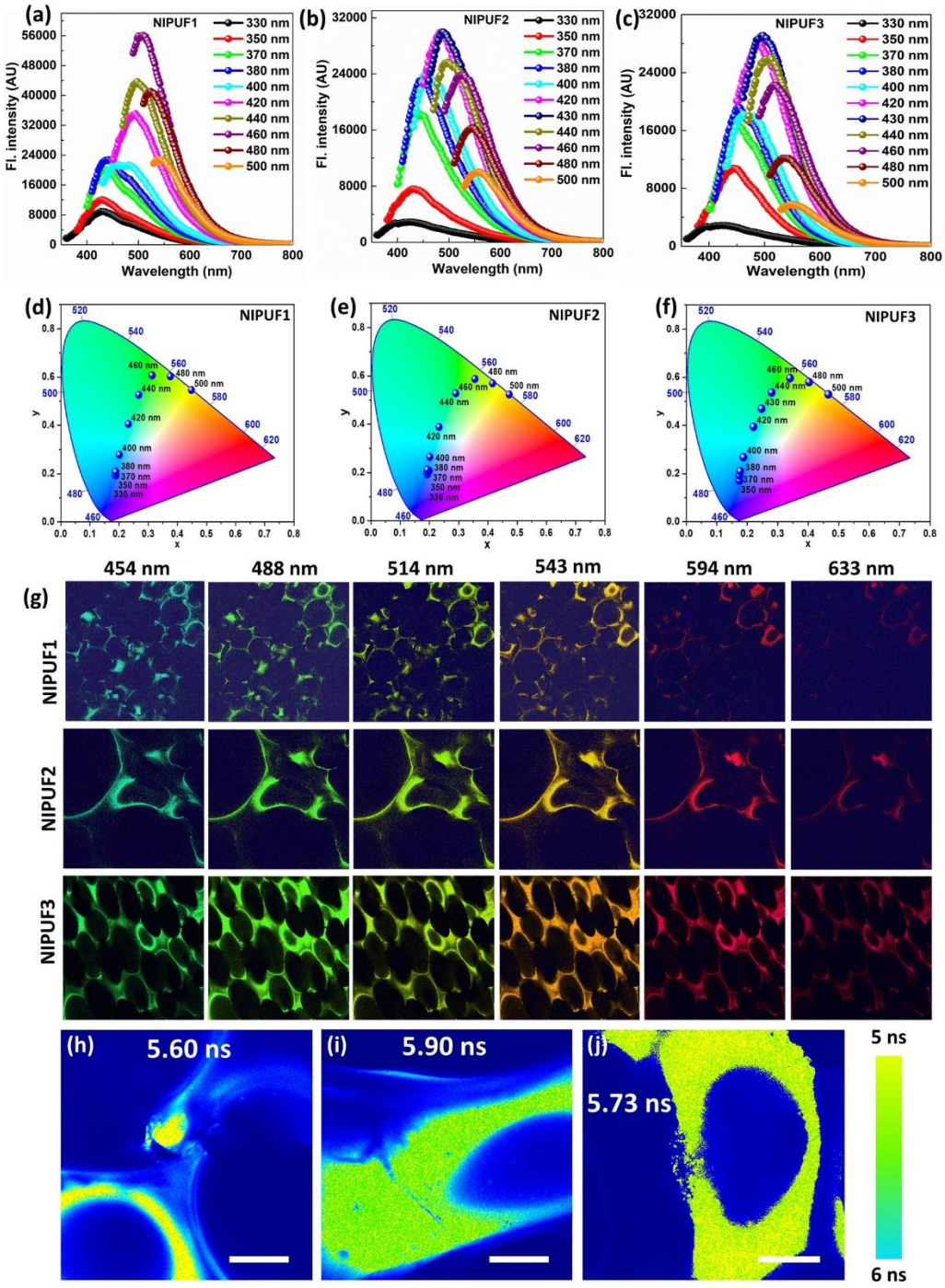

Published in : Angewandte Chemie International Edition (2025), vol. 64, n°1, e202413605
DOI: https://doi.org/10.1002/anie.202413605
Status : Postprint (Author's version)

2.2. CAPTURING AND SENSING OF GASEOUS FORMALDEHYDE

NIPUF3 was investigated for gaseous FA capturing (Figure 4a), following standard protocols.[52,61] In brief, in a plastic container were introduced the NIPU foam and an emission vial containing an aqueous solution of FA. The container was hermetically sealed, and the system was allowed to equilibrate for different period of times. The FA concentration in the solution was then assessed after different exposition times by the colorimetric NASH test by UV-Vis spectroscopy at 412 nm (Figure S27 and see ESI on page S78 for details). The content of captured FA was then easily obtained from this value and taking into account FA saturating the container atmosphere. Figure 4b shows a decrease in the FA concentration from 0.9 to 0.3 mM in the presence of NIPUF3 after 7 days of exposition. For sake of comparison, the FA capturing ability of NIPUF2 was also assessed, and demonstrated to be slightly lower. The main important difference between the two foams was that captured FA was not released from NIPUF3 foam in contrast to NIPUF2 when performing release experiments (Figure 4c). This was the result of the free amine groups in NIPUF3 that reacted with FA to form stable adducts (Figure 4a), as demonstrated by the model reaction between PEI and FA (Figure S28 and S29), as well as ATR-IR studies carried out on the foams (Figure S30) (see ESI for details).[52-56] The chemical modification of NIPUF3 during FA capturing also affected its thermal properties, with a T_g value that increased significantly from —2.95 to 8.50 °C after FA capturing (Figure S31). This is in line with the introduction of rigid structures upon reaction of FA with free amines of the foams that decreased the chain mobility, consequently increasing T_g. Beside, no change in the foam morphology was detected after FA capture (Figure S32). While the distribution of the nonconventional fluorescent chromophores in the polymer matrix as well as their fluorescence lifetime (5.74 ns *vs* 5.73 ns) were not significantly affected by FA capturing (Figure 4d and Figure S33), their fluorescence emission was strongly altered as shown in Figure 4e,f. The change of the chemical structure of the foam by FA condensation with amine groups was associated to a maximum fluorescence signal at 450 nm (λ_{ex} = 380 nm) and 495 nm (λ_{ex} = 430 nm) in NIPUF3 that was red shifted to 490 nm (λ_{ex} = 380 nm) and 525 nm (λ_{ex} = 430 nm) in the FA-captured foam (FA-NIPUF3). The covalently crosslinked structure produced aggregates of higher order and increased the foam crosslinking degree, both being responsible for red-shifted emissions. This FA capturing was also associated to a decrease in fluorescence intensity due to the lowering of free —NH_2 available for hydrogen bonding (Figure 4e,f). The FA capturing was thus easily observed by the foam fluorescence colour change from cyan to green (λ_{ex} = 454 nm) (Figure 4g), enabling to detect FA.

Published in : Angewandte Chemie International Edition (2025), vol. 64, n°1, e202413605
DOI: https://doi.org/10.1002/anie.202413605
Status : Postprint (Author's version)

***Figure 3**. (a) Schematic presentation of NIPU foam showing all possible modes of hydrogen bonding interactions (simplified for clarity); (b) HOMOs and LUMOs of NIPUF1 (1b + 2b + 3), NIPUF2 (1a + 2a + 3) and NIPUF3 (1a + 2a + 3 + PEI) in ground state and first excited state; (c) simple Jablonski diagram for fluorescence showing different energy levels; (d) small (1a + 2a + 3), moderate (2 ×(1a + 2a + 3)) and large (3×(1a + 2a + 3)) aggregates of NIPUF2 showing the decreasing HOMO-LUMO energy gaps.*

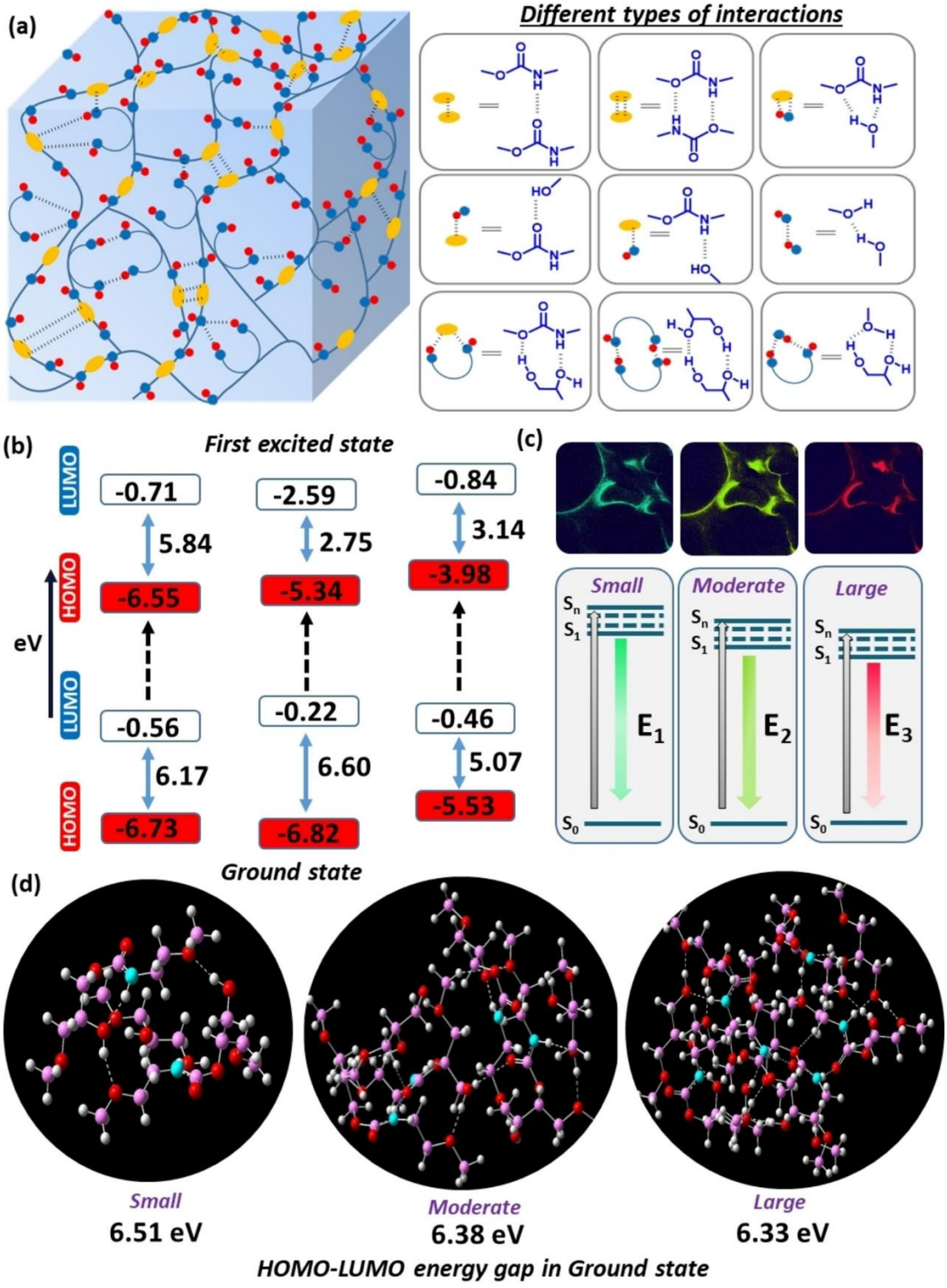

Published in : Angewandte Chemie International Edition (2025), vol. 64, n°1, e202413605
DOI: https://doi.org/10.1002/anie.202413605
Status : Postprint (Author's version)

***Figure 4**. (a) Scheme showing the formaldehyde capture; (b) gaseous formaldehyde capture by foams placed in a closed vial containing 0.9 mM FA (results normalized to blank); (c) formaldehyde release experiment from the foams; (d) fluorescence lifetime imaging microscopy (FLIM) image of FA-NIPUF3, scale bar = 100 µm, used laser = 455 nm; fluorescence spectra of NIPUF3 and FA-NIPUF3 at excitation wavelengths (e) 380 nm and (f) 430 nm; (g) change in fluorescence color from cyan in NIPUF3 to green in FA-NIPUF3 after binding with formaldehyde, scale bar = 200 µm.*

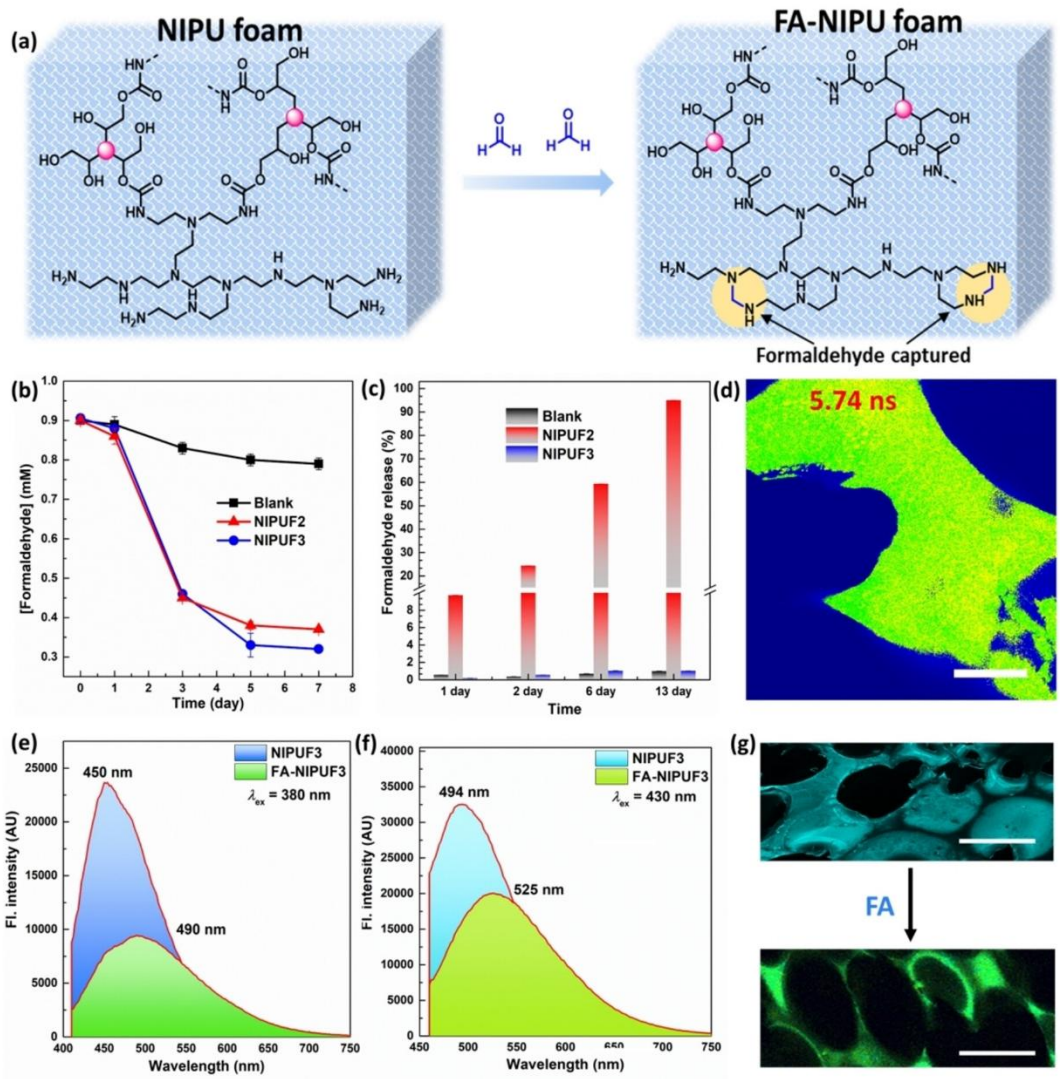

2.3. METAL IONS SENSING AND QUANTIFICATION

NIPUF3 was then evaluated for sensing various metal ions by exploiting their pending amine groups, well-known to bind to many types of metal cations (Figure S34). The binding affinities of NIPUF3 with various cations (K^+, Ca^{2+}, Mg^{2+}, Ba^{2+}, Zn^{2+}, Hg^{2+}, Mn^{2+}, Co^{2+}, Ni^{2+}, Al^{3+}, Fe^{3+}, Fe^{2+}, Cu^{2+}) of their water-soluble salts were tested at room temperature in aqueous solution (pH = 7.0-7.6) (Figure S35a,c,e,g,i,k; see ESI, section 6 for experimental details). It was found that NIPUF3 bonded selectively (fluorescence selectivity) to Cu^{2+}, Fe^{2+}, Fe^{3+} and Hg^{2+} as confirmed by the high quenching

Published in : Angewandte Chemie International Edition (2025), vol. 64, n°1, e202413605
DOI: https://doi.org/10.1002/anie.202413605
Status : Postprint (Author's version)

efficiencies of their corresponding emission spectra (λ_{ex} = 380 nm), i.e. 90.5%, 85.6%, 74.3% and 73.2%, respectively (Figure S35b) and showed similar order of selectivity for all emission spectra (λ_{ex} = 400-430 nm). They were not considered to be significant for the other cations (Figure S35b,d,f,h,j,l). The fluorescence intensity of NIPUF3 recorded at λ_{ex} of 380 and 430 nm decreased gradually by increasing the metal ions concentration in solution (Figure 5a-c). Although Hg^{2+} showed effective quenching at higher concentrations, the changes in fluorescence intensity were however random with high standard error and the results were not fully reproducible (Figure S39a-d). Thus, Hg^{2+} could only be sensed but not quantified.

The fluorescence quenching was utilized to quantify the metal ions (Fe^{2+}, Cu^{2+} and Fe^{3+}) with a high precision. For that purpose, calibration plots were created by measuring the relative fluorescence ($F_0|F$) at various concentrations (within 0-150 ppm range) at two excitation wavelengths, i.e. λ_{ex} = 380 and 430 nm. An inductively coupled plasma optical emission spectrometer was used to quantify the metal ions in the solution. For Fe^{2+}, Cu^{2+} and Fe^{3+}, linear calibrations were recorded up to 88.8, 70.4 and 78.8 ppm, respectively, with excellent goodness-of-fit (adj. R^2 >0.98) when λ_{ex} = 380 nm was used (Figures 5d-f). Similar linear calibrations curves were obtained at λ_{ex} = 430 nm (Figure S36-S38). The binding constants (K_{SV}) of metal cations to NIPUF3 were calculated by the Stern-Volmer (SV) equation following the standard procedure (see ESI for details), and their values are summarized in Figure 5j. The highest binding constant was noted for Fe^{2+} (K_{SV} = 139838 M^{-1} at λ_{ex} = 380 nm), and lower ones were obtained for the two other metal cations, i.e. 5599 and 6061 M^{-1} for Cu^{2+} and Fe^{3+}, respectively (Figure 5d-f and Figure S36b-S38b). Values in the same range were calculated from the fluorescence data recorded at λ_{ex} = 430 nm.

The limits of detection (LODs) of the metal cations were calculated to be 0.66, 0.76 and 0.18 µM (λ_{ex} = 380 nm) for Fe^{2+}, Cu^{2+} and Fe^{3+}, respectively (Figure 5j and Figure S40a-c). As illustrated in Table S6, the binding performance and limits of detection of NIPUF3 were as good or even much better than those reported for polyurethane foams containing conventional fluorescent probes. The exclusion performance of NIPUF3 was then performed at various higher concentrations and the data fitted with Langmuir model (Figure S41a-c, Table S7, see ESI for details), which enabled to determine the maximum binding performance to the different metals, i.e. 196.6, 81.0 and 60.2 $mg.g^{-1}$ for Fe^{2+}, Cu^{2+} and Fe^{3+}, respectively (Figure S41a-c). This confirmed the chemical nature of interactions between metal ions and NIPUF3, thus the static nature of binding. The strong binding of metal ions in ground state via complexation was further evidenced by the change of foam color, visible by naked eyes, when contacted with the metal cation.

Indeed, the foam changed from yellowish white to blue when binding with Cu^{2+} (Figure S42). Some dynamic quenching in binding might also contribute to the on-off metal ions sensing in the linear nature of fluorescence quenching in lower range of concentration. This was evidenced by the altered fluorescence lifetimes in metal ions loaded samples by FLIM analysis. Metal complexation increased the fluorescence lifetime from 5.73 ns (NIPUF3), to 6.40 ns (Fe^{2+}-NIPUF3), 5.85 ns (Cu^{2+}-NIPUF3), 6.07 ns (Fe^{3+}-NIPUF3) and 6.20 ns (Hg^{2+}-NIPUF3), confirming the dynamic quenching (Figure 5g-i and Figure S43a-e). ATR-IR spectroscopy also evidenced the interactions of the metal cations with oxygen (—CH_2OH, > CHOH, —O—) and nitrogen (—COONH—, —NH_2) donors of NIPUF3 (Figure S44a

Published in : Angewandte Chemie International Edition (2025), vol. 64, n°1, e202413605
DOI: https://doi.org/10.1002/anie.202413605
Status : Postprint (Author's version)

and see ESI for details). These interactions were further supported by the optimized structures modeled by DFT calculations (Figures S45-S47). The positive frequencies confirmed the existence of these types of complexes as shown in Table S8, and the strong previous interactions were confirmed by short bond lengths (< 2 Å; Figures S45-S47). The nitrogen donors of PEI in NIPUF3 interacted with metal ions too with short bond lengths. Moreover, metal binding to NIPUF3 increased the foam rigidity by physical crosslinking as attested by the increase of T_g value from -2.95 °C for NIPUF3 to 13.15, 12.50, 9.10 and 8.60 °C in Fe^{2+}-NIPUF3, Cu^{2+}-NIPUF3, Fe^{3+}-NIPUF3 and Hg^{2+}-NIPUF3, respectively (Figure 6a-c and Figure S48a). Importantly, this binding did not significantly affect the foam thermal stability (Figure S44b) nor its morphology (Figure 6d-f). The homogeneous deposition of the metal cations on the surface of the foam pores were visualized by scanning electron microcopy energy dispersive X-ray (SEM-EDX) mapping (Figure 6g-i and Figure S48), and was confirmed by the homogeneous distribution of the chromophores in FLIM (Figure 5g-i). We have also tested the performance of NIPUF3 for Cu^{2+} sensing in the presence of different counter-anions (OAc^-, Br^- and SO_4^{2-}). NIPUF3 showed binding performance of 14.7, 16.0 and 20.5 mg/g for $Cu(OAc)_2$, $CuBr_2$ and $CuSO_4$, respectively, at initial concentration of 80 ppm. The counter-ions thus slightly influenced the binding performance of the foam. However, an identical fluorescence quenching was monitored at the same concentration of Cu^{2+} within the foams irrespective of the anions (Figure S49).

As a proof of concept, these metal ions were released on demand by simply dipping the foams in acidic water (pH = 1.80) that protonated the amines responsible for metal binding. While moderate release efficiencies were obtained for Fe^{2+} (50 %) and Fe^{3+} (60 %), more than 90 % of bonded Cu^{2+} was released under these non-optimized conditions (Figure S50). NIPUF was thus not only able to sense and quantify these metal cations, but also to capture and release them on demand, which is highly appealing for waste water purification applications for instance.

Finally, in order to further illustrate the interest to use NIPU foams for metal ion capturing and sensing, we compared the binding performance and sensing ability of foamed and non-foamed NIPUF3. Binding performances of 2.00, 2.42 and 0.90 mg/g for Fe^{2+}, Cu^{2+} and Fe^{3+}, respectively, were measured for initial concentrations in metal cations of 100 ppm for non-foamed NIPUF3. For sake of comparison, under identical experimental conditions, NIPUF3 foam showed a higher performance (140 mg/g for Fe^{2+}, 27 mg/g for Cu^{2+} and 16 mg/g for Fe^{3+}). Figure S51a shows that the emission fluorescence of non-foamed NIPUF3 was quenched by increasing the content of Cu^{2+} cation similarly to the foam, however the F_0/F plot *vs* Cu^{2+} concentration was linear on a shorter concentration range (i.e. over 25 ppm compared to 70.4 ppm for the foam) (Figure S51b). Sensing with the non-foamed material was thus less sensitive.

Published in : Angewandte Chemie International Edition (2025), vol. 64, n°1, e202413605
DOI: https://doi.org/10.1002/anie.202413605
Status : Postprint (Author's version)

***Figure 5**. Fluorescence intensities of NIPUF3 loaded with different concentration of (a) Fe^{2+} ion (0—82.8 ppm), (b) Cu^{2+} ion (0-126.2 ppm) and (c) Fe^{3+} ion (0-100.3 ppm) at λ_{ex} = 380 nm; relative fluorescence versus concentration plots of NIPUF3 in presence of (d) Fe^{2+} ion (88.8 ppm), (e) Cu^{2+} ion (70.4 ppm) and (f) Fe^{3+} ion (78.8 ppm) at λ_{ex}=380 nm; the used mass of NIPUF3 = 0.05 g, the exact concentration of metal ions was determined by an inductively coupled plasma optical emission spectrometer (ICP-OES: Varian 720-ES) at respective wavelengths, the experiment was performed twice with three replicates; fluorescence lifetime imaging microscopy (FLIM) images showing the lifetime distributions of (g) Fe^{2+}-NIPUF3, (h) Cu^{2+}-NIPUF3 and (i) Fe^{3+}-NIPUF3 using the laser source of 455 nm, jet colormap is used for generating the image colormap, scale bar = 100 μm; the used threshold minimum/maximum = 100/5 000; (j) table showing fluorescence lifetime, binding constants, limit of detections and binding performances of metal ions loaded samples.*

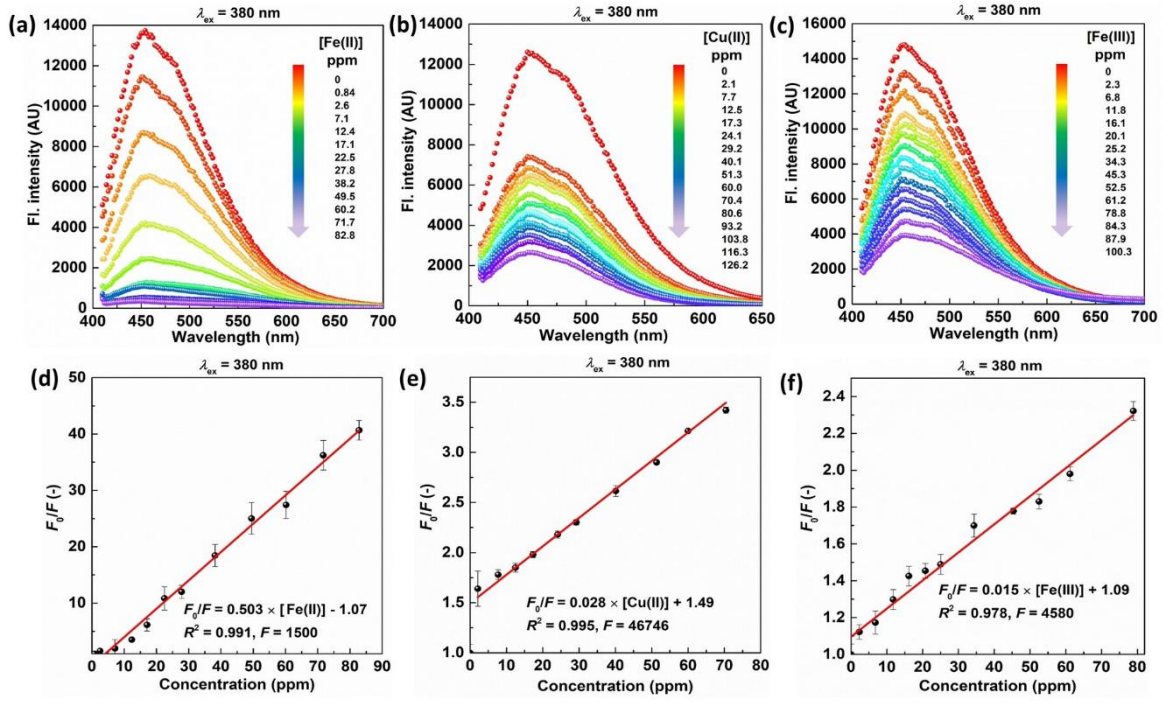

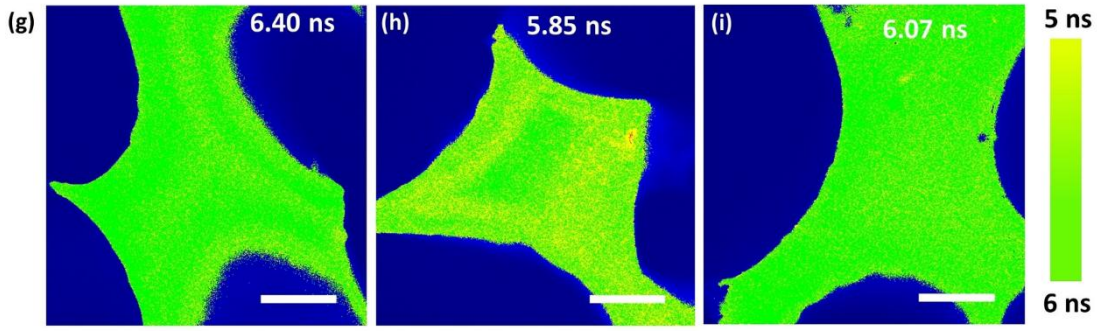

(j)

Parameters	Fe^{2+}-NIPUF3	Cu^{2+}-NIPUF3	Fe^{3+}-NIPUF3
Fluorescence lifetime (ns)	6.40	5.85	6.07
Binding constants (K_{SV}/ M^{-1}) at λ_{ex} = 380 nm	139838	5599	6061
Binding constants (K_{SV}/ M^{-1}) at λ_{ex} = 430 nm	160411	5799	7475
Limit of detection (μM)	0.66	0.76	0.18
Binding performance (mg g^{-1})	196.63	81.03	60.27

Published in : Angewandte Chemie International Edition (2025), vol. 64, n°1, e202413605
DOI: https://doi.org/10.1002/anie.202413605
Status : Postprint (Author's version)

2.4. ANTIBIOTIC SENSING AND QUANTIFICATION

Tetracycline (TCY) is a low cost widely used bacteriostatic antibiotic, active against a broad range of pathogenic bacteria (e.g. *Streptococcus, Staphylococcus*, etc.).[62,63] Its excessive consumption (about 5000 metric tons per year) to treat bacterial infections in animals, fishes and humans is responsible for waste water contamination by TCY residues, which has accelerated the emergence of antibiotic-resistant bacteria.[64-66] Therefore, it is urgent to develop efficient tools to detect and quantify TCY in waste-water. Herein, we demonstrate that NIPUF3 is a highly sensitive and selective ratiometric fluorescent sensor for TCY. For this study, eight relevant families of antibiotics were here evaluated (Scheme S1 and Figure S52,S53). After contacted the foam with the different antibiotics (concentration of 1 mM), the emission intensity of the dried foams was only slightly decreased (λ_{ex} = 380 nm) for seven of them, with no shift in their maximum emission wavelength. Remarkably, after contacting with TCY, the intensity of the fluorescence emission spectrum strongly decreased, and its maximum emission was significantly red-shifted (518 *vs* 452 nm; Figure S53h). The same observation was done at λ_{ex} = 430 nm (548 *vs* 494 nm) (Figure S53i). The signature peak of the TCY/NIPUF3 interaction at 516 nm (λ_{ex} = 380 nm) was also retained when the NIPUF3 was added in a solution of a mixture of the eight antibiotics (identical concentrations of 1.25×10^{-4} M), enabling the selective TCY detection (Figure S54).

When NIPUF3 was contacted with increasing concentrations of TCY, the foam was characterized by a multicolor photoluminescence as visualised from blue to yellow under the UV-lamp of 366 nm (Figure 7d). This was further evidenced by the appearance of the typical emission signal of the TCY/NIPUF3 interaction at 516 nm (λ_{ex} = 380 nm) that increased with the TCY concentration, and therefore tuned the global fluorescence emission (Figure 7a). The ratio of fluorescence (F_{516}/F_{450}) showed a best-fitted linear relation with [TCY] = 0-100 µM (R^2 = 0.9973; F = 3200) (Figure 7c), with a lower limit of detection (LOD, S/N=3) of 3.17×10^{-8} M. This low LOD was inspiring compared to other similar fluorescence materials for TCY detection (Figure S55; Table S9), supporting the excellent sensitivity of NIPUF3 for TCY sensing.

To further demonstrate the utility of our foam for the facile and fast TCY detection and quantification, we designed a smartphone-compatible gadget composed of a smartphone loaded with an accessible RGB colour scanning application (available on app stores of iOS or android) (Figure S56). The variations of the fluorescence colour (from blue-to-green-to-yellow, λ_{ex} = 366 nm) of NIPUF3 enabled the immediate and on-the-spot visual detection of TCY antibiotic from aqueous solution. The blue, green and yellow colours along with their transition colours of the fluorescent images were directly scanned with the RGB application (Figure 7e). Based on the ratio of converted G/B values and TCY concentrations, a calibration curve was established and employed for the facile quantification of TCY (Figure 7f). Once the foam was loaded with TCY, its quantification using the portable smartphone-compatible device was complete in few minutes, demonstrating the tremendous potential of NIPUF3 as a photoluminescence device for trace detection of TCY in water.

The fluorescence lifetimes of neat NIPUF3 and NIPUF3 loaded with different TCY contents (by contacting the foam with different TCY concentrations of 10^{-9}, 10^{-6} and 10^{-3} M) were determined as 5.73, 5.77, 5.11 and 2.00 ns, respectively (Figure 7g-i and Figure S57). At the lower TCY concentration,

Published in : Angewandte Chemie International Edition (2025), vol. 64, n°1, e202413605
DOI: https://doi.org/10.1002/anie.202413605
Status : Postprint (Author's version)

the mechanism of binding was static quenching as confirmed from the almost unaltered fluorescence lifetimes compared to neat NIPUF3 (Figure 7g). However, at higher concentrations, the lowering in lifetimes up to 5.11 and 2.00 ns indicated a combination of static and dynamic quenching.[67,68] The lowering in lifetimes with increasing TCY content indicated predominant interactions in the ground and excited states due to the formation of strong TCY/NIPUF3 complex driven by hydrogen bonding as confirmed by DFT calculations on model compounds (see ESI: Figures S58-S62 for details). TCY loaded NIPUF3 was characterized by an increased T_g (11.90 *vs* — 2.95 °C), confirming the strong interaction of TCY to the polymer backbone (Figure S63).

***Figure 6**. DSC plots of (a) Fe^{2+}-NIPUF3, (b) Cu^{2+}-NIPUF3 and (c) Fe^{3+}-NIPUF3; SEM photomicrographs of (d) Fe^{2+}-NIPUF3, (e) Cu^{2+}-NIPUF3 and (f) Fe^{3+}-NIPUF3, scale bar = 2.0 mm; EDX mapping of (g) Fe^{2+}-NIPUF3, (h) Cu^{2+}-NIPUF3 and (i) Fe^{3+}-NIPUF3.*

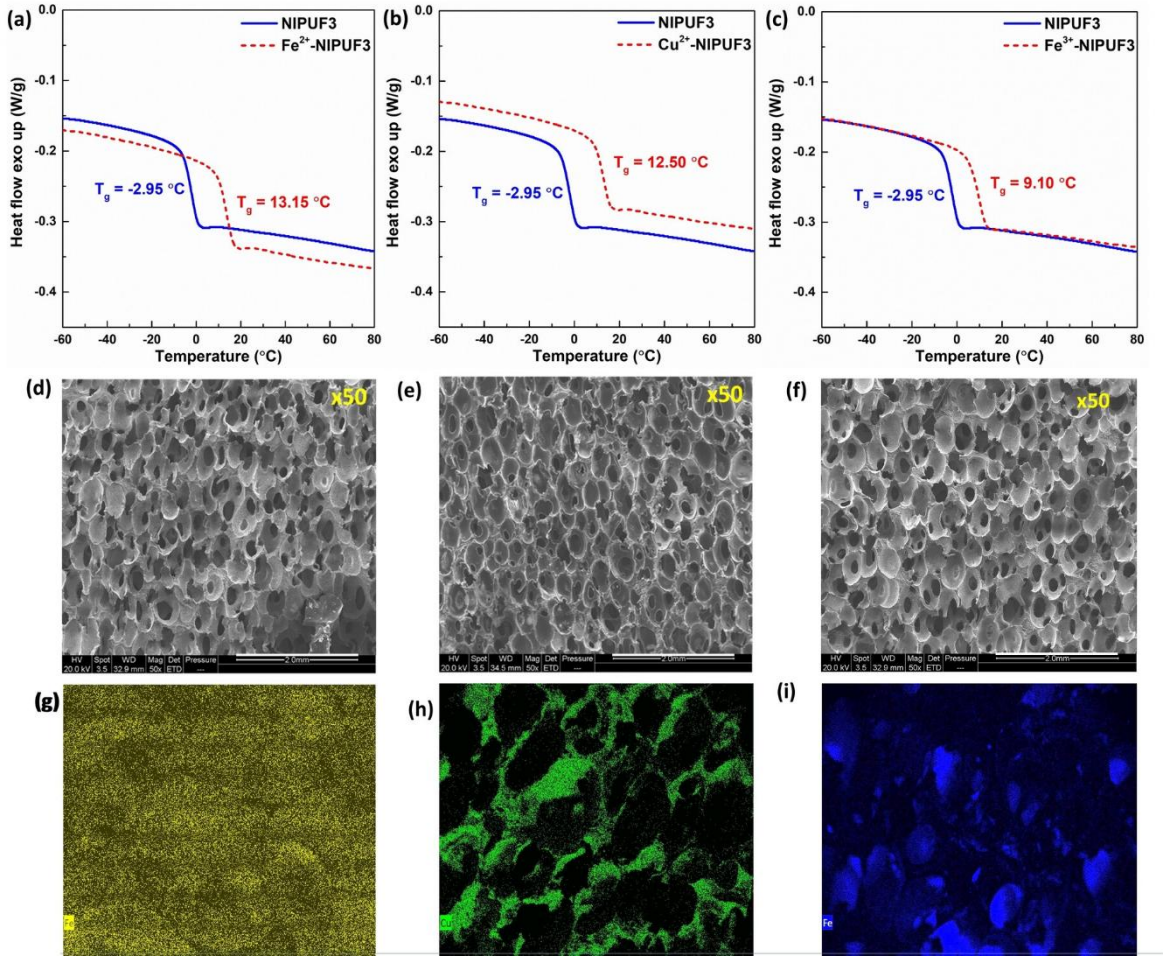

Published in : Angewandte Chemie International Edition (2025), vol. 64, n°1, e202413605
DOI: https://doi.org/10.1002/anie.202413605
Status : Postprint (Author's version)

***Figure 7**. (a) Fluorescence spectra of NIPUF3 in presence of different concentration of TCY (0-100 μM) using λ_{ex} = 380 nm; (b) chemical structure of tetracycline; (c) relative fluorescence (F_{516}/F_{450}) of NIPUF3 in presence of different concentrations of TCY (0-100 μM); (d) photographic images of TCY loaded NIPUF3 foams showing color transitions in presence of different concentrations of TCY (0-150 μM) under the UV-lamp (λ = 366 nm); (e) smartphone-compatible gadget for scanometric monitoring of TCY using an accessible RGB color scanning application showing R, G and B components; (f) calibration plot producing via mobile app for TCY quantification by NIPUF3; fluorescence lifetime imaging microscopy (FLIM) images of (g) 1×10^{-9} M, (h) 1×10^{-6} M and (i) 1×10^{-3} M ofTCY loaded NIPUF3 using the laser source of 455 nm, jet colormap is used for generating the image colormap, scale bar = 100 μm; the used threshold minimum/maximum = 100/5000.*

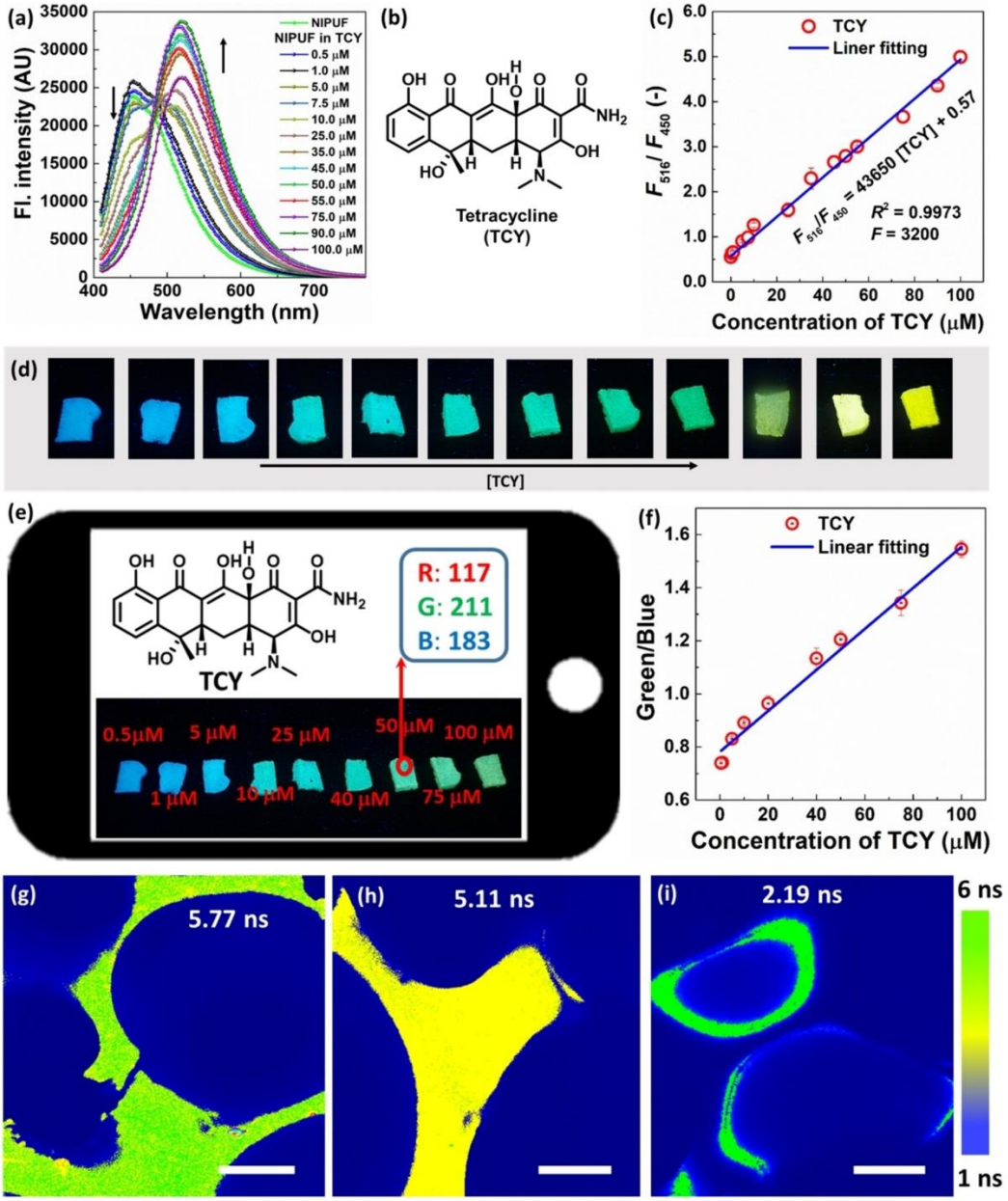

Published in : Angewandte Chemie International Edition (2025), vol. 64, n°1, e202413605
DOI: https://doi.org/10.1002/anie.202413605
Status : Postprint (Author's version)

3. Conclusion

In this work, non-isocyanate polyurethane foams (NIPUFs), prepared by the facile, up scalable water-induced selfblowing process, present a nonconventional fluorescence behaviour, i.e. they are intrinsically fluorescent with a multicolor emission without requiring the utilization of any conventional fluorophores. This fluorescence behaviour is based on clusteroluminescence originating from multiple hydrogen bonding and hetero-atomic sub-luminophores, thus from aggregation-induced emission luminogens that are naturally present in these isocyanate-free polyurethane foams. The identification of chromophores was executed by theoretical analyses optimizing model compounds and aggregates in ground and first excited states. These NIPU foams differentiate themselves from conventional PU foams by the high concentration of hydroxyl groups that strongly participate to the clusteroluminescence.

The luminescence property of the foams was then exploited for capturing-sensing an emblematic indoor air pollutant (gaseous formaldehyde), but also for detecting and quantifying various metal ions (Fe^{2+}, Cu^{2+}, Fe^{3+}, Hg^{2+}). The unique multicolor photoluminescent foam property was also utilized for the selective sensing and quantification of an antibiotic (tetracycline) by using a smartphone loaded with an accessible RGB colour scanning application. By scanning the fluorescent images of the foams contacted with tetracycline, the antibiotic quantification was facile and complete in few minutes based on the ratio of G/B values reported to a pre-established calibration curve. The binding mechanism with formaldehyde, metal ions, and tetracycline were discussed by analysing the loaded foams by FLIM, DSC, SEM and EDX analyses, and was supported by DFT calculations of the clusters/aggregates on model compounds. This work illustrates that easily accessible non-conventional fluorescent NIPU foams characterized by a modular emission wavelength have an enormous potential for multiple substrates detection and, in some cases, quantification. They are attractive, more sustainable alternatives to conventional PU foams containing conventional fluorescent probes.

Published in : Angewandte Chemie International Edition (2025), vol. 64, n°1, e202413605
DOI: https://doi.org/10.1002/anie.202413605
Status : Postprint (Author's version)

Author Contributions

M.M. and C.D. conceived the project. M.M. conducted all experiments and data analysis under the supervision of C.D. and the guidance of M.B. M.B. provided the experimental protocols for preparing the foams. B.G. prepared the cyclic carbonates needed to synthesize the foams. M.V. assisted M.M. in monitoring the fluorescent behaviour of the foams under the supervision of M.G. M.M. performed and analyzed all DFT calculations. M.M. provided the first draft of the paper and revised the document following the suggestions of the co-authors. All authors contributed to editing the manuscript.

Acknowledgements

MM is grateful to the Sector Council for Research and Valorisation in Science and Techniques of University of Liege (ULiège) for funding. This research is supported by the ULiège under Special Funds for Research, IPD-STEMA Programme. Computational resources have been provided by the Consortium des Équipements de Calcul Intensif (CÉCI), funded by the Fonds de la Recherche Scientifique de Belgique (F.R.S.-FNRS) under Grant No. 2.5020.11 and by the Walloon Region. The authors acknowledge the Robotein platform of the BE Instruct-ERIC Center for providing access to the Fluorescence microplate reader. We gratefully acknowledge Yuxing Wang and Dr. Sebastien Rochat (University of Bristol, UK) for carrying out fluorescence quantum yield measurements, and Prof. Jelle Hendrix (Hasselt University, Belgium) for performing the FLIM studies. CD is FNRS Research Director and thanks the Fonds de la Recherche Scientifique (F.R.S.-FNRS) for funding. CD, BG and MB thank the Region Wallonne for funding the Win2Wal project "ECOFOAM" (convention 2010130) and the FRFS-WEL T Advanced Grant project of CD (project CHEMISTRY, convention WEL-T-CR-2023A). A preprint of this article appeared on ChemRxiv at https://doi.org/10.26434/chemrxiv-2024-kbcr5.

Data Availability Statement

All data that support the findings of this study are found in the main manuscript or in Supporting Information.

Published in : Angewandte Chemie International Edition (2025), vol. 64, n°1, e202413605
DOI: https://doi.org/10.1002/anie.202413605
Status : Postprint (Author's version)

References

[1] S. Wang, H. Li, H. Huang, X. Cao, X. Chen, D. Cao, Chem. Soc. Rev. 2022, 51, 2031.

[2] Q. Huang, K. Otake, S. Kitagawa, Angew. Chem. Int. Ed. 2023, 62, e202310225.

[3] A. P. Vijayan, K. Ramakrishnan, J. G. Elambalassery, ACS Appl. Polym. Mater. 2024, 6, 3975.

[4] J. Gayle, S. Roy, S. Gupta, S. Hassan, A. Rao, P. G. Demingos, K. Miller, G. Guo, X. Wang, A. Garg, C. V. Singh, R. Vajtai, J. T. Robinson, P. M. Ajayan, ACS Appl. Mater. Interfaces 2024, 16, 2726.

[5] Q. Liu, Q. Sun, J. Shen, H. Li, Y. Zhang, W. Chen, S. Yu, X. Li, Y. Chen, Coord. Chem. Rev. 2023, 482, 215078.

[6] S. Fajal, S. Dutta, S. K. Ghosh, Mater. Horiz. 2023, 10, 4083.

[7] W. He, J. Duan, H. Liu, C. Qian, M. Zhu, W. Zhang, Y. Liao, Prog. Polym. Sci. 2024, 148, 101770.

[8] F. Monie, B. Grignard, J. Thomassin, R. Mereau, T. Tassaing, C. Jerome, C. Detrembleur, Angew. Chem. Int. Ed. 2020, 132, 17181.

[9] Z. Zhou, Q. Wang, Z. Zeng, L. Yang, X. Ding, N. Lin, Z. Cheng, Anal. Methods 2013, 5, 6045.

[10] Y. Su, D. Zhang, P. Jia, W. Gao, Y. Li, J. He, C. Wang, X. Zheng, Q. Yang, C. Yang, Eur. Polym. J. 2019, 112, 461.

[11] Y. Chen, Y. Wu, Y. Zhu, S. Tian, Polym. Int. 2022, 71, 169.

[12] Z.-X. Fan, Q.-H. Zhao, S. Wang, Y. Bai, P.-P. Wang, J.-J. Li, Z.-W. Chu, G.-H. Chen, RSC Adv. 2016, 6, 26950.

[13] Z. Chu, Z. Fan, X. Zhang, X. Tan, D. Li, G. Chen, Q. Zhao, Sensors 2018, 18, 1565.

[14] V. V. Apyari, V. V. Arkhipova, M. V. Gorbunova, P. A. Volkov, A. I. Isachenko, S. G. Dmitrienko, Y. A. Zolotov, Talanta 2016, 161, 780.

[15] Y. Yu, J. Wang, J. Lian, X. Cheng, RSC Adv. 2014, 4, 18222.

[16] Y. Su, D. Zhang, P. Jia, W. Gao, Y. Li, Z. Bai, X. Liu, Q. Deng, J. Xu, C. Yang, Spectrochim. Acta Part A 2019, 217, 86.

[17] M. Amela-Cortes, S. Paofai, S. Cordier, H. Folliot, Y. Molard, Chem. Commun. 2015, 51, 8177.

[18] S. Wang, K. Zhou, X. Lyu, H. Li, Z. Qiu, Z. Zhao, B. Z. Tang, Chem. Biomed. Imaging 2023, 1, 509.

[19] H. Li, B. Jin, Y. Wang, B. Deng, D. Wang, B. Z. Tang, Adv. Mater. 2023, 35, 2210085.

[20] X. Cai, B. Liu, Angew. Chem. Int. Ed. 2020, 59, 9868.

[21] F. Fang, L. Zhu, M. Li, Y. Song, M. Sun, D. Zhao, J. Zhang, Adv. Sci. 2021, 8, 2102970.

[22] M. Gao, B. Z. Tang, ACS Sens. 2017, 2, 1382.

[23] B. Liu, B. Chu, Y.-L. Wang, L.-F. Hu, S. Hu, X.-H. Zhang, Green Chem. 2021, 23, 422.

[24] B. Liu, Y.-L. Wang, W. Bai, J.-T. Xu, Z.-K. Xu, K. Yang, Y.-Z. Yang, X.-H. Zhang, B.-Y. Du, J. Mater. Chem. C 2017, 5, 4892.

[25] A. Qin, J. W. Y. Lam, B. Z. Tang, Prog. Polym. Sci. 2012, 37, 182.

[26] J. Luo, Z. Xie, J. W. Y. Lam, L. Cheng, B. Z. Tang, H. Chen, C. Qiu, H. S. Kwok, X. Zhan, Y. Liu, D. Zhu, Chem. Commun. 2001, 1740.

[27] J. Deng, H. Jia, W. Xie, H. Wu, J. Li, H. Wang, Macromol. Chem. Phys. 2022, 223, 2100425.

[28] D. A. Tomalia, B. Klajnert-Maculewicz, K. A.-M. Johnson, H. F. Brinkman, A. Janaszewska, D. M. Hedstrand, Prog. Polym. Sci. 2019, 90, 35.

[29] S. Tang, T. Yang, Z. Zhao, T. Zhu, Q. Zhang, W. Hou, W. Z. Yuan, Chem. Soc. Rev. 2021, 50, 12616.

[30] X. Ji, W. Tian, K. Jin, H. Diao, X. Huang, G. Song, J. Zhang, Nat. Commun. 2022, 13, 3717.

[31] G. Caminati, N. J. Turro, D. A. Tomalia, J. Am. Chem. Soc. 1990, 112, 8515.

[32] Q. Li, X. Wang, Q. Huang, Z. Li, B. Z. Tang, S. Mao, Nat. Commun. 2023, 14, 409.

[33] M. Mahapatra, A. Dutta, J. S. D. Roy, M. Mitra, S. Mahalanobish, M. H. Sanfui, S. Banerjee, P. K. Chattopadhyay, P. C. Sil, N. R. Singha, Adv. Healthcare Mater. 2019, 8, 1900980.

[34] M. Mahapatra, A. Dutta, J. S. D. Roy, U. Das, S. Banerjee, S. Dey, P. K. Chattopadhyay, D. K. Maiti, N. R. Singha, Chem. Eur. J. 2020, 26, 502.

[35] M. Mahapatra, A. Dutta, J. S. D. Roy, M. Deb, U. Das, S. Banerjee, S. Dey, P. K. Chattopadhyay, D. K. Maiti, N. R. Singha, Langmuir 2020, 36, 6178.

[36] R. Ye, Y. Liu, H. Zhang, H. Su, Y. Zhang, L. Xu, R. Hu, R. T. K. Kwok, K. S. Wong, J. W. Y. Lam, W. A. Goddard, B. Z. Tang, Polym. Chem. 2017, 8, 1722.

[37] J. Yan, X. Wang, J. Xiong, L. Wang, D. Pan, Y. Xu, M. Yang, J. Chem. Eng. 2022, 428, 132142.

[38] M. Sun, C.-Y. Hong, C.-Y. Pan, J. Am. Chem. Soc. 2012, 134, 20581.

[39] X. Zhou, W. Luo, H. Nie, L. Xu, R. Hu, Z. Zhao, A. Qin, B. Z. Tang, J. Mater. Chem. C 2017, 5, 4775.

[40] H. Zhang, Z. Zhao, P. R. McGonigal, R. Ye, S. Liu, J. W. Y. Lam, R. T. K. Kwok, W. Z. Yuan, J. Xie, A. L. Rogach, B. Z. Tang, Mater. Today 2020, 32, 275.

[41] N. Jiang, C.-Y. Zhu, K.-X. Li, Y.-H. Xu, M. R. Bryce, Macromolécules 2024, 10.1021/acs.macromol.4c00186.

[42] Official Journal of the European Union, L252, Https://Eur-Lex. Europa.Eu/Legal-Content/EN/TXT/PDF/?Uri= OJ: L:2020 :252:FULL&from=EN.

[43] C. Zhou, T. Xie, R. Zhou, C. O. Trindle, Y. Tikman, X. Zhang, G. Zhang, ACS Appl. Mater. Interfaces 2015, 7, 17209.

[44] Y. Ou, Z. Zhang, Z. Tang, Z. Yang, Y. Zhang, L. Tao, T. Wang, Q. Wang, S. Chen, J. Polym. Sci. 2023, 61, 1360.

[45] Z. Feng, W. Zhao, Z. Liang, Y. Lv, F. Xiang, D. Sun, C. Xiong, C. Duan, L. Dai, Y. Ni, ACS Appl. Mater. Interfaces 2020, 12, 11005.

[46] W. Xu, B. Liu, X. Cai, M. Zhang, X. Zhang, P. Yu, J. Appl. Polym. Sci. 2018, 135, 46723.

[47] J. J. Warner, P. Wang, W. M. Mellor, H. H. Hwang, J. H. Park, S.-H. Pyo, S. Chen, Polym. Chem. 2019, 10, 4665.

[48] M. Bourguignon, B. Grignard, C. Detrembleur, Angew. Chem. Int. Ed. 2022, 61, e202213422.

[49] M. Zhao, F. Yang, Y. Xue, D. Xiao, Y. Guo, ChemPhysChem 2014, 15, 950.

[50] X.-N. Li, Z.-J. Wu, Z.-J. Si, H.-J. Zhang, L. Zhou, X.-J. Liu, Inorg. Chem. 2009, 48, 7740.

[51] A. Douvali, A. C. Tsipis, S. V. Eliseeva, S. Petoud, G. S. Papaefstathiou, C. D. Malliakas, I. Papadas, G. S. Armatas, I. Margiolaki, M. G. Kanatzidis, T. Lazarides, M. J. Manos, Angew. Chem. Int. Ed. 2015, 127, 1671.

Published in : Angewandte Chemie International Edition (2025), vol. 64, n°1, e202413605
DOI: https://doi.org/10.1002/anie.202413605
Status : Postprint (Author's version)

[52] M. Bourguignon, B. Grignard, C. Detrembleur, ACS Appl. Mater. Interfaces 2021, 13, 54396.

[53] A. Ghani, Z. Ashaari, P. Bawon, S. H. Lee, Building Environ. 2018, 142, 188.

[54] B. Robert, G. Nallathambi, J. Polym. Res. 2022, 29, 500.

[55] C. Zhang, X. Wang, J. Lin, B. Ding, J. Yu, N. Pan, Sens. Actuators B 2011, 152, 316.

[56] N. Wang, X. Wang, Y. Jia, X. Li, J. Yu, B. Ding, Carbohydr. Polym. 2014, 108, 192.

[57] Z. M. Ayalew, X. Guo, X. Zhang, J. Hazard. Mater. 2022, 8, 100158.

[58] W. Maketon, C. Z. Zenner, K. L. Ogden, Environ. Sci. Technol. 2008, 42, 2124.

[59] F. Bucatariu, C.-A. Ghiorghita, M.-M. Zaharia, S. Schwarz, F. Simon, M. Mihai, ACS Appl. Mater. Interfaces 2020, 12, 37585.

[60] H. H. P. Yiu, L. Bouffier, P. Boldrin, J. Long, J. B. Claridge, M. J. Rosseinsky, Langmuir 2013, 29, 11354.

[61] C. Resetco, D. Frank, T. Dikić, S. Claessens, T. Verbrugge, F. E. Du Prez, Eur. Polym. J. 2016, 82, 166.

[62] C. M. T. Spahn, C. D. Prescott, J. Mol. Med. 1996, 74, 423.

[63] D. Schnappinger, W. Hillen, Arch. Microbiol. 1996, 165, 359.

[64] K. D. Wasch, L. Okerman, H. D. Brabander, J. V. Hoof, S. Croubels, P. D. Backer, Analyst 1998, 123, 2737.

[65] S. Croubels, C. Van Peteghem, W. Baeyens, Analyst 1994, 119, 2713.

[66] M. Jeon, I. Rhee Paeng, Anal. Chim. Acta 2008, 626, 180.

[67] A. S. Tanwar, R. Parui, R. Garai, M. A. Chanu, P. K. Iyer, ACS Meas. Sci. Au 2022, 2, 23.

[68] D. A. Olley, E. J. Wren, G. Vamvounis, M. J. Fernee, X. Wang, P. L. Burn, P. Meredith, P. E. Shaw, Chem. Mater. 2011, 23, 789.